THE JOURNAL OF PHYSICAL CHEMISTRY B

Article

pubs.acs.org/JPCB

Molecular Dynamics Study of Anhydrous Lamellar Structures of Synthetic Glycolipids: Effects of Chain Branching and Disaccharide Headgroup

Vijayan Manickam Achari,[†] Hock Seng Nguan,[†] Thorsten Heidelberg,[†] Richard A. Bryce,*[,‡] and Rauzah Hashim*[,†,§]

[†]Department of Chemistry, University of Malaya, 50603 Kuala Lumpur, Malaysia

[‡]School of Pharmacy and Pharmaceutical Sciences, University of Manchester, Manchester, M13 9PT, U.K.

[§]Kavli Institute of Theoretical Physics China, Chinese Academy of Sciences, Beijing 100190, China

Supporting Information

ABSTRACT: Glycolipids form materials of considerable potential for a wide range of surfactant and thin film applications. Understanding the effect of glycolipid covalent structure on the properties of their thermotropic and lyotropic assemblies is a key step toward rational design of new glycolipid-based materials. Here, we perform molecular dynamics simulations of anhydrous bilayers of dodecyl β-maltoside, dodecyl β-cellobioside, dodecyl β-isomaltoside, and a $C_{12}C_{10}$ branched β-maltoside. Specifically, we examine the consequences of chain branching and headgroup identity on the structure and dynamics of the lamellar assemblies. Chain branching of the glycolipid leads to measurable differences in the dimensions and interactions of the lamellar assembly, as well as a more fluid-like hydrophobic chain region. Substitution of the maltosyl headgroup of βMal-C_{12} by an isomaltosyl moiety leads to a significant decrease in bilayer spacing as well as a markedly altered pattern of inter-headgroup hydrogen bonding. The distinctive simulated structures of the two regioisomers provide insight into the difference of ~90 °C in their observed clearing temperatures. For all four simulated glycolipid systems, with the exception of the *sn*-2 chain of the branched maltoside, the alkyl chains are ordered and exhibit a distinct tilt, consistent with recent crystallographic analysis of a branched chain Guerbet glycoside. These insights into structure−property relationships from simulation provide an important molecular basis for future design of synthetic glycolipid materials.

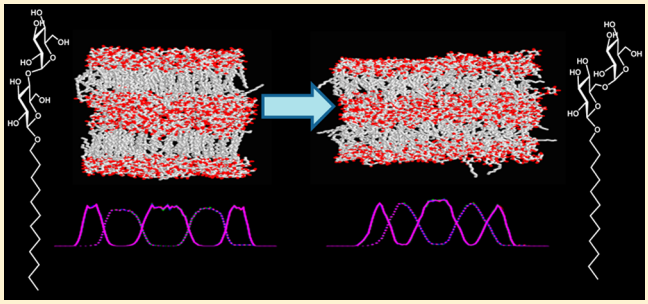

INTRODUCTION

Alkyl glycosides are a family of glycolipids comprising a carbohydrate headgroup linked via a glycosidic bond to an alkyl chain. Naturally occurring glycosides exist in both prokaryotic and eukaryotic cell membranes[1] and play an important role in many cellular processes.[2] Unfortunately, these natural glycosides are difficult to extract in high yield and purity, thus limiting the ability to explore their biological properties.[3] Consequently, synthetic glycolipids are highly sought after, especially those with promising properties that mimic the natural ones.[3−5] For example, industrially produced dodecyl β-maltoside (βMal-C_{12}) has been used in the purification and stabilization of proteins, like RNA polymerase, and the detection of protein−lipid interactions.[6−8]

Given the potential for drawing on the very large library of possible saccharide headgroups naturally available, there is considerable scope for tuning the properties of synthetic glycolipids, in both thermotropic and lyotropic phases, to tackle scientifically and commercially important problems, such as those found in thin film and surfactant applications. However, the relationship between headgroup and physicochemical properties of these materials is rather exquisite.[9] For example, the phase diagrams of anomers αMal-C_{12} and βMal-C_{12} are very different, as is that found for C4 epimers, alkyl β-glucoside and β-galactoside.[10] In cell membranes, detailed glycolipid structure is known to affect its function; in one case, the presence of cholesterol within the membrane induces a tilt in glycolipid headgroup, resulting in loss of access for ligand binding, suggesting that lipid "allostery" can regulate membrane recognition processes.[11]

Consequently, there is a need to understand at the molecular level the relationship between glycolipid structure and the properties of their assemblies. Computational simulation constitutes a powerful tool for characterization of the molecular-level structure and dynamics of such systems. There exist relatively few simulation studies on glycolipid materials[12−15] when compared to the extensive work on phospholipids (for example, see refs 16−24). However, the

Received: March 9, 2012
Revised: August 30, 2012

   dx.doi.org/10.1021/jp302292s | *J. Phys. Chem. B* XXXX, XXX, XXX−XXX

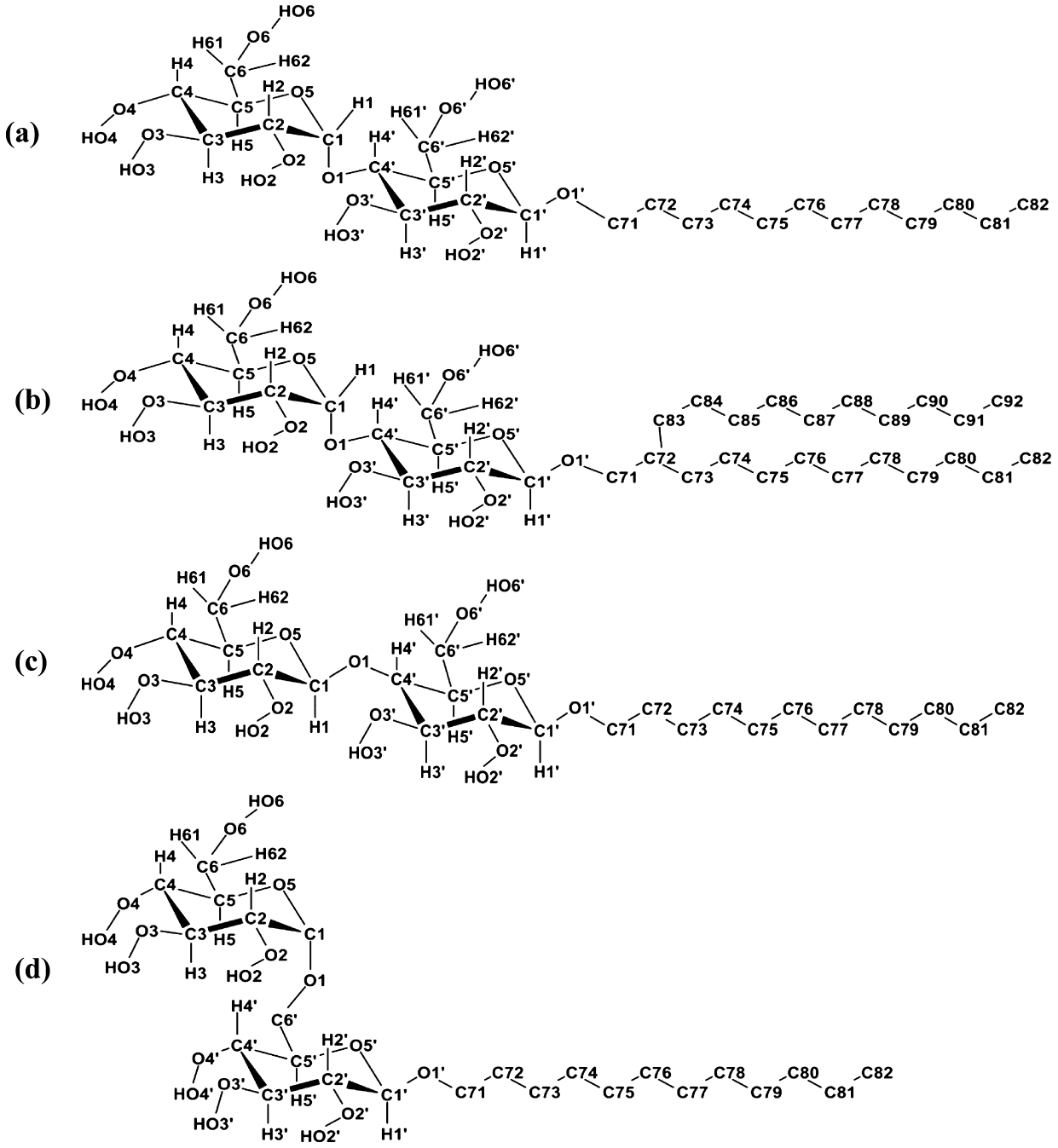

Figure 1. Glycosides simulated: (a) βMal-C_{12}; (b) βBCMal-$C_{12}C_{10}$; (c) βCel-C_{12}; (d) βIsoMal-C_{12}. Note: In part d, H61′ and H62′ atoms were omitted for clarity; also, to avoid conflict with sugar atom labeling, each glycolipid's main alkyl chain is labeled from C71 to C82, starting from glycosidic oxygen, and the branched chain from C83 to C92.

glycolipid simulation studies that have been performed explore both naturally occurring[11,13−15,25,26] and synthetic glycolipid systems.[12,16,27]

Using molecular dynamics (MD) simulations, we characterize here the structure and dynamics of four synthetic glycoside materials in an anhydrous bilayer arrangement. Four disaccharide glycosides were chosen to explore the effect of both sugar headgroup identity and tail branching on lamellar structure: these glycolipids are dodecyl β-maltoside (βMal-C_{12}, Figure 1a), a branched chain maltoside (βBCMal-$C_{12}C_{10}$, Figure 1b), dodecyl β-cellobioside (βCel-C_{12}, Figure 1c), and dodecyl β-isomaltoside (βIsoMal-C_{12}, Figure 1d). Experimentally, the anhydrous states of these systems are difficult to achieve due to the presence of the hygroscopic sugar group.[28] Nevertheless, recent studies indicate that the anhydrous states of these systems form self-assemblies.[28,29] Thus, our simulations aim to yield valuable insights into the molecular structure and dynamics of these interesting and potentially very useful glycolipid materials.

COMPUTATIONAL METHODOLOGY

Model Construction. Initial coordinates of βMal-C_{12}, βBCMal-$C_{12}C_{10}$, βCel-C_{12}, and βIsoMal-C_{12} were built via the HyperChem package.[30] Following the IUPAC nomenclature, glycosidic angles, φ and ψ, of disaccharide headgroups are

dx.doi.org/10.1021/jp302292s | J. Phys. Chem. B XXXX, XXX, XXX−XXX

defined as H1−C1−O1−C4′ and C1−O1−C4′−H4′, respectively.[31,32] Initial values of φ and ψ for βMal-C_{12} and βBCMal-C_{12} were taken from Ott et al.,[33] while for cellobioside and isomaltoside, these were taken from Ham et al.[34] and Jeffrey et al.,[35] respectively (see Table S1, Supporting Information).

These structures were geometry optimized within HyperChem. The *crystal builder* facility in HyperChem was then used to arrange the molecules in an 8 × 8 monolayer. In our previous bilayer simulations of alkyl monosaccharide glycolipids,[27] the chain region was found at the end of the simulation to be slightly tilted, which is consistent with the fact that at 27 °C, according to the phase diagram,[10] the system exists in either the L_C (lamellar crystal) phase or L_β (gel) phase but not the L_α (fluid lamellar) phase; the latter phase comprises melted alkyl chains and corresponds to smectic A in thermotropic liquid crystal nomenclature.[36] This phase occurs at much higher temperatures for the monoalkylated systems. Only the branched chain compounds give a thermotropic fluid lamellar phase at room temperature.[37] X-ray studies on the L_C phase for both βMal-C_{14} and βMal-C_{16} have demonstrated these phases to be tilted and interdigitated.[28] In light of this, the initial configuration of the present model has the lipid molecules tilted about 15° relative to the bilayer normal.

Each 8 × 8 monolayer was geometry optimized and rotated by 180° and shifted to form a bilayer with the tail group of the molecules pointing toward each other at the center of the bilayer and the headgroups facing opposite directions. Then, the single bilayer was replicated to form a second bilayer, providing a large lamellar simulation cell of 256 lipids.

Simulation Details. The four glycoside lamellar systems were then equilibrated using AMBER9,[38] with parameters from the *ff99*[39] and GLYCAM_06d[40] force fields to model the tails and head groups, respectively. A nonbond cutoff of 9 Å was applied in calculating nonelectrostatic interactions, and long-range electrostatic interactions were treated using the particle mesh Ewald method.[41,42] The SHAKE algorithm[43] was used to constrain covalent bonds involving hydrogen. The systems were heated gradually over 2 ns from 0 to 27 °C in the NVT ensemble, using the Andersen thermostat (τ_P = 0.5 ps)[44] and a 1 fs time step. Subsequently, the systems were equilibrated under conditions of constant pressure *NpT*, initially with isotropic scaling of box dimensions (50 ns) followed by anisotropic scaling (100 ns).[45] The Berendsen algorithm was used to achieve pressure coupling, with a coupling constant of 1 ps and for anisotropic coupling, a compressibility of 4.5 × 10^{-5}/bar. Discussed below, βIsoMal-C_{12} appeared to compact more than the other three systems; therefore, a more extensive isotropic simulation was performed for 80 ns, then followed by 100 ns of anisotropic simulation. As discussed below, the final 40 ns of the 150 or 180 ns glycolipid trajectories were used for analysis. Coordinates were archived every 5 ps.

Analysis. Hydrogen bond analysis was performed using the *ptraj* module of AMBER, defining the O−O distance to be ≤4 Å and an angle cutoff of 120° from linearity.[27] Density profiles were calculated along the bilayer normal, taking the center of the bilayer as the origin. This distribution function $g(z)$ is calculated from the number density, $\rho(x,y,z)$, given as

$$N = \iiint \rho(x, y, z)\, dx\, dy\, dz \tag{1}$$

where N is the total number of atoms. Along the z-direction, we define $g(z)$ as

$$g(z) = \rho(z)/\rho = (N(z)V)/(A\Delta z N) \tag{2}$$

where A is the bilayer area, Δz is the bin size along the z-axis, and V is the volume.

The degree of ordering in the chain region may be estimated from the order parameter, S. This is derived from a 3 × 3 Saupe ordering tensor, **S**, whose ijth element is given as

$$S_{ij} = 1/2(\overline{3\cos\theta_i \cos\theta_j} - \delta_{ij}) \tag{3}$$

where θ_i is the angle between the ith molecular axis and the bilayer normal and the bar denotes time averaging.[46] For definition of an alkyl chain order parameter, we follow van der Ploeg and Berendsen:[24] the molecular axes for the nth methylene group are defined by the H−H vector (x), the bisectrix of the H−C_n−H angle (y), and the vector C_{n-1} to C_{n+1} (z). From symmetry arguments, the tensor **S** is diagonal and S_{zz} represents the chain order parameter. S_{zz} takes a value of unity if the average orientation is parallel to the bilayer normal (i.e., fully ordered), −1/2 if it is perpendicular to the normal, and zero if the system is completely disordered. Related to deuterium NMR experiments, another informative order parameter is S_{CD} (=S_{CH}), given as

$$S_{CD} = 2/3S_{xx} + 1/3S_{yy} \tag{4}$$

where S_{xx} and S_{yy} are the order parameters in the x and y directions, respectively. We also calculate the chain tilt vector **T** and the corresponding average tilt angle θ after van der Ploeg et al.[24] Thus, **T** is defined as

$$\mathbf{T} = \frac{1}{N}\sum_{i=1}^{N} \mathbf{R}_i \tag{5}$$

where $\mathbf{R}_i$ is a normalized vector. Various definitions of $\mathbf{R}_i$ have been proposed.[24,47] Here, we calculate tilt angle and tilt vector via four methods:

Method A. The $\mathbf{R}_i$ vector for the single chain lipid is defined from the midpoint of C71−C72 to that of C80−C81 (Figure 1). For the *sn*-1 chain of βBCMal-$C_{12}C_{10}$, $\mathbf{R}_i$ connects the midpoint of C72−C73 and C80−C81, while, for *sn*-2, it links C72−C83 to C90−C91 (Figure 1). **T** is averaged over the four layers indiscriminately.

Method B. $\mathbf{R}_i$ is defined as in method A. **T** is averaged over the first layer only.

Method C. As in method B, the average **T** is defined over the first layer only. However, unlike methods A and B, $\mathbf{R}_i$ is defined for single chain lipids from the midpoint of C74−C75 to that of C80−C81. For the *sn*-1 chain of βBCMal-$C_{12}C_{10}$, $\mathbf{R}_i$ connects the midpoint of C74−C75 and C80−C81, while, for *sn*-2, this was taken from the midpoint of C84−C85 to that of C90−C91.

Method D. This is similar to method B, but the tail vector is defined from C73−C74 and C79−C80 for the single alkyl chain. For the *sn*-1 chain of βBCMal-$C_{12}C_{10}$, $\mathbf{R}_i$ connects the midpoint of C73−C74 and C79−C80, while, for *sn*-2, this was taken from the midpoint of C83−C84 to that of C89−C90.

RESULTS

Bilayer Structure. We have performed MD simulations of four glycolipid assemblies, βMal-C_{12}, βBCMal-$C_{12}C_{10}$, βCel-C_{12}, and βIsoMal-C_{12}. On the basis of local density profiles (LDPs) from 20 ns block averages over the final 100 ns,[48] it can be seen that the lamellar structures for each glycolipid system have converged (Figure 2). We take the last 40 ns of these

dx.doi.org/10.1021/jp302292s | J. Phys. Chem. B XXXX, XXX, XXX−XXX

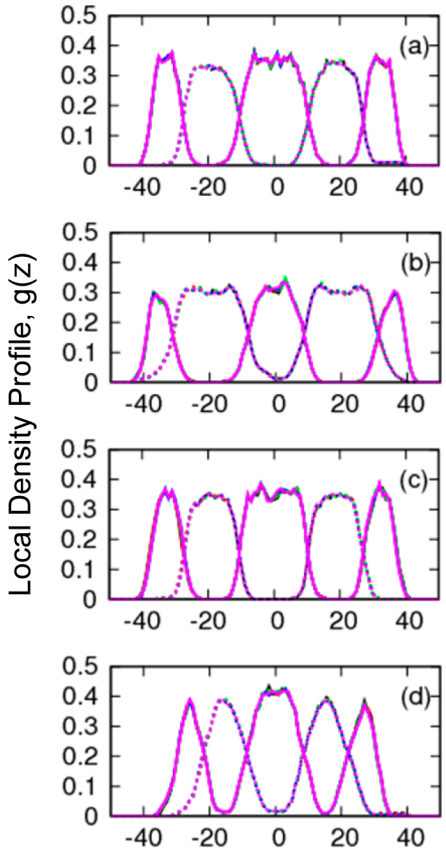

Figure 2. Local density profiles over 100 ns for (a) βMal-C_{12}, (b) βBCMal-$C_{12}C_{10}$, (c) βCel-C_{12}, and (d) βIsoMal-C_{12} for headgroup (solid line) and tail (dotted line). LDPs are computed for 1−20 ns (red), 21−40 ns (black), 41−60 ns (green), 61−80 ns (blue), and 81−100 ns (magenta).

trajectories for performing subsequent structural and dynamic analyses. On the basis of these equilibrated trajectories, the average surface area per headgroup was calculated. As expected, these computed areas are very similar for βMal-C_{12} and βCel-C_{12}, with values of 38.8 and 38.7 Å^2, respectively (Table 1). This is in reasonable agreement with the value of 43 Å^2 for βMal-C_{12} based on X-ray crystallographic layer spacing.[19] Interestingly, the calculated headgroup surface area for βIsoMal-C_{12}, the third of the single chain glycosides studied here, is some 10 Å^2 larger, at 48.6 Å^2 (Table 1); this is an increase of 26% from its regioisomer, βMal-C_{12}. The area value is similar to that of the branched chain lipid βBCMal-$C_{12}C_{10}$, where the headgroup surface area increases further to 51.9 Å^2 (Table 1), 34% larger than βMal-C_{12}. This is presumably to accommodate strain introduced by the larger splay of the chain region.

Table 1. Headgroup Surface Area per Lipid (A), Bilayer Spacing (d), and Average Volume of Simulation Box ($\langle V \rangle$)

	Calculated		
glycolipid	A (Å^2)	d (Å)	$\langle V \rangle$ (10^3 Å^3)
βMal-C_{12}	38.8 ± 0.2	32.9 ± 0.5	183.2 ± 0.6
βBCMal-$C_{12}C_{10}$	51.9 ± 0.2	36.1 ± 0.2	258.2 ± 0.8
βCel-C_{12}	38.7 ± 0.1	32.3 ± 0.2	181.9 ± 0.5
βIsoMal-C_{12}	48.6 ± 0.2	26.6 ± 0.6	185.3 ± 0.6
	Experiment		
			ref
βMal-C_{12}(L_α)	43 (20 °C)	33.5 (20 °C), 41.5 (80 °C)	10, 19
βMal-$C_{12}C_8$(L_α)	53 (25 °C)	36.2 (25 °C)	19
βMal-$C_{14}C_{10}$(L_α)	58 (25 °C)	36.9 (25 °C)	19
βMal-C_{14} (L_C)		38.2 (25 °C)	28
βMal-C_{16} (L_C)		41.2 (25 °C)	28

In addition to the highest predicted surface area of the three single chain glycolipid systems, the βIsoMal-C_{12} bilayer exhibits the largest degree of compaction, as can be seen from the overlap of hydrophilic and hydrophobic domains in the local density profile (Figure 2d). The isomaltoside d spacing is 26.6 Å, some 19 and 18% less than the d values observed for βMal-C_{12} and βCel-C_{12}, respectively (Table 1).

From visual inspection of MD configurations (Figure 3), the compression of d spacing in the βIsoMal-C_{12} system is evident (Figure 3d). As before for headgroup surface area, the calculated bilayer distances are similar for βMal-C_{12} (32.9 ± 0.5 Å) and βCel-C_{12} (32.3 ± 0.2 Å); the spacing for βMal-C_{12} agrees well with the value of 33.5 Å at 20 °C from small-angle X-ray diffraction.[10] Interestingly, the average volumes of the simulation box $\langle V \rangle$ are similar for the three monoalkylated lipids, βMal-, βCel-, and βIsoMal-C_{12} (Table 1). For βIsoMal-C_{12}, this observation results from a 19% reduction in the z-direction of the bilayer normal (Figure 3), compensated by an increase in the xy area of the bilayer to result in an overall volume comparable to the other two isomers.

We note that the simulated average d-spacing value for βBCMal-$C_{12}C_{10}$ is 36.1 Å. This is larger than the values of the single chain glycolipids here, and is similar to the experimental values of Guerbet maltosides with $C_{12}C_8$ and $C_{14}C_{10}$ branches, which have d-spacings of 36.2 and 36.9 Å, respectively, at 25 °C (Table 1).[19] As a consequence of this branching, βBCMal-$C_{12}C_{10}$ packs the least well of the four glycolipid simulations, with the largest average volume, of 258.2 Å^3 (Table 1).

Chain Structure. We now characterize the simulated alkyl chain behavior of the four glycolipid assemblies. The C−D bond order parameter $-\langle S_{CD} \rangle$ is given as a function of methylene carbon position in Figure 4. Here, we observe the overall trend is comparable for βMal-C_{12} and βCel-C_{12}; i.e., $-\langle S_{CD} \rangle$ profiles display a maximum at the eighth methylene of the chain (i.e., position C78 as defined in Figure 1). This parabolic chain ordering profile mirrors those obtained from previous simulations of chains of decanoate, DPPC, and DMPC bilayers.[23,24,47] Here, $-\langle S_{CD} \rangle$ indicates that the alkyl chains of βCel-C_{12} are on average more aligned (more ordered) with the bilayer than those of the maltoside, with peak values (corresponding to the eighth methylene unit) of 0.25 for βMal-C_{12} and 0.34 for βCel-C_{12} (Figure 4).

A cross-section through a typical MD snapshot for each of the four assemblies exemplifies chain tilting behavior (Figure S2, Supporting Information). However, for βIsoMal-C_{12}, $-\langle S_{CD} \rangle$ decreases monotonically across the chain order, to a more disordered state at the tail end (Figure 4). For βBCMal-$C_{12}C_{10}$, from the values of $-\langle S_{CD} \rangle$ across chain length, the shorter sn-2 (C_{10}) chain is less ordered than the sn-1 (C_{12}) chain (Figure 4). The maxima for the two chains are found at the seventh and ninth methlyenes for sn-1 and sn-2, respectively (Figure 4). Interestingly, in contrast to the other chains, the sn-2 chain possesses a $-\langle S_{CD} \rangle$ with a small negative value, closer to the headgroup, indicating that the C−D bond is ordered to some degree parallel with respect to the bilayer normal. These results are in qualitative agreement with those measured for other lipid systems, for example, 1-13-methylpentadecanoyl-2-

dx.doi.org/10.1021/jp302292s | J. Phys. Chem. B XXXX, XXX, XXX−XXX

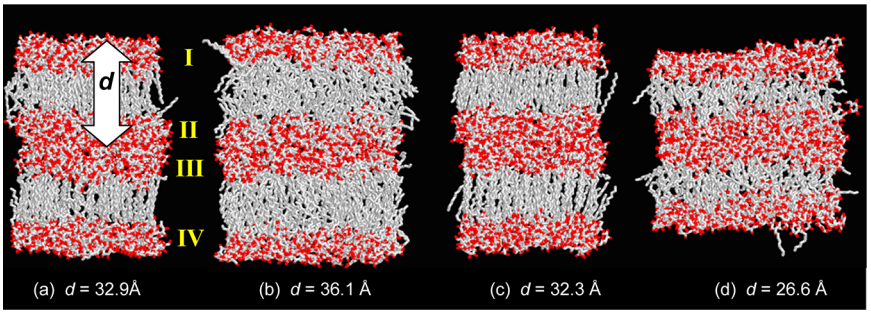

Figure 3. Molecular dynamics configuration at t = 40 ns of lamellar assemblies and average interlayer spacings d of (a) βMal-C_{12}, (b) βBCMal-$C_{12}C_{10}$, (c) βCel-C_{12}, and (d) βIsoMal-C_{12}. Layers labeled I–IV.

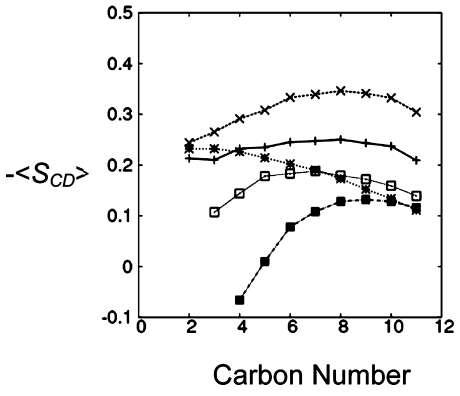

Figure 4. The average order parameters, $-\langle S_{CD}\rangle$, for βMal-C_{12} (+), βBCMal-$C_{12}C_{10}$(*sn*-1) (□), βBCMal-$C_{12}C_{10}$(*sn*-2) (■), βCel-C_{12} (×), and βIsoMal-C_{12} (∗). Connecting lines drawn only as a guide.

palmitoyl-phosphatidylcholine (13-MpPPC) and dimyristoyl-phosphatidylcholine (DMPC) by MD simulations[49,50] and experiment.[51,52] Obviously, these results differ quantitatively because of differing lipid structure and environment (anhydrous vs aqueous conditions).

In order to quantitatively evaluate the degree of tilting in the bilayer assemblies, we calculate an ensemble-averaged tilt angle θ and tilt vector |**T**| for the four lamellar systems. Here we use four different methods, labeled A–D (see Methods); these approaches vary in their definitions of chain vector and degree of averaging (see Methods).

Method A, which indiscriminately averages tilt over the four layers of each system, yields average tilt angles close to 90° and tilt vectors close to zero, for each of the four glycolipid systems (Table 2). This indicates no net tilt over the four layers. The exception is the *sn*-2 chain of βBCMal-$C_{12}C_{10}$ which has a |**T**| value of 0.42. The surprisingly high nonzero value of the tilt modulus is due to the x–y components of the tilt vector being nonzero on average, suggesting that, while the z-component is not correlated on average across the four layers, the x–y component is fairly correlated.

Methods B–D define the tilt orientation of a single lipid leaflet. Here, for the monoalkylated systems of βMal-C_{12}, βCel-C_{12}, and βIsoMalC_{12}, we observe a broad consensus of 32–41° in tilt angle θ (or an average of 37°), with a corresponding tilt vector modulus in the range of ∼0.8–0.9 (Table 2). Interestingly, the value does not seem to vary strongly with headgroup identity. However, the actual value of θ seems rather high when compared with the recently reported value of 12° from X-ray studies on the L_C phase of a branched chain Guerbet glucoside.[53] For βBCMal-$C_{12}C_{10}$, the longer *sn*-1 chain is more tilted than the chains of the monoalkylated lipids, with an average tilt angle of 51°. However, the *sn*-2 chain appears to tilt yet more heavily, with a θ value of ∼60–70° and |**T**| of ∼0.5 (Table 2). We also note a level of negative correlation between the instantaneous values of θ and |**T**|. This behavior is illustrated for βMal-C_{12} using method B (Figure 5), although

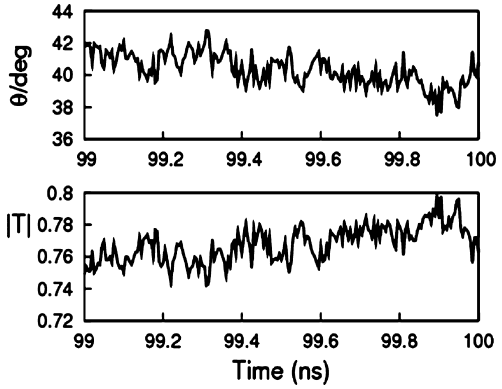

Figure 5. Short dynamic behavior for tilt vector and tilt angle θ of βMal-C_{12}.

the observation appears to hold across method and lipid system; the complete set of angular correlation plots between

Table 2. Average Chain Tilt Angles and Vectors by Methods A–D

	average tilt angle θ by method				average tilt vector |**T**| by method			
lipid	A	B	C	D	A	B	C	D
βMalC_{12}	89.0 ± 0.4	38 ± 1	41 ± 2	38 ± 2	0.05 ± 0.02	0.79 ± 0.02	0.76 ± 0.03	0.91 ± 0.01
βBCMal-C_{12}	91.0 ± 0.4	45 ± 2	54 ± 2	54 ± 1	0.17 ± 0.02	0.73 ± 0.02	0.60 ± 0.03	0.62 ± 0.01
βBCMal-C_{10}	89.3 ± 0.9	70 ± 1	63 ± 1	66 ± 1	0.42 ± 0.02	0.49 ± 0.03	0.50 ± 0.03	0.50 ± 0.01
βCel-C_{12}	90.7 ± 0.3	36 ± 2	38 ± 2	32 ± 2	0.04 ± 0.01	0.83 ± 0.01	0.81 ± 0.02	0.87 ± 0.01
βIsoMal-C_{12}	89.3 ± 0.4	35 ± 2	39 ± 2	37 ± 2	0.05 ± 0.01	0.82 ± 0.02	0.78 ± 0.02	0.79 ± 0.02

dx.doi.org/10.1021/jp302292s | J. Phys. Chem. B XXXX, XXX, XXX–XXX

normalized molecular vector and average tilt is given in Figure S3 (Supporting Information). This behavior is reasonable, given that, as the angular tilt increases, the correlation between tilt directions must decrease for the monoalkylated lipids. Finally, on the basis of method C, we consider the distribution of tilt angle, layer-by-layer, for the four glycolipid systems (Figure S4, Supporting Information). It is evident that these distributions are skewed rather than Gaussian. The maxima of these distributions provide one further estimate of tilt angle (Table 3).

Table 3. Layer and Overall Tilt Angles θ (in deg), Estimated from Maxima of Tilt Angle Distributions (Corrected Values in Parentheses), via Method C

layer	I	II	III	IV	av
βMal-C_{12}	17	161 (19)	18	162 (18)	18
βBCMal-C_{12} *sn*-1	20	160 (20)	38	152 (28)	27
βBCMal-C_{10} *sn*-2	23	138 (42)	31	155 (25)	30
βCel-C_{12}	11	164 (16)	12	167 (13)	13
βIsoMal-C_{12}	30	156 (24)	25	157 (23)	26

According to this measure, the tilt angles for layers I–IV of βMal-C_{12} are 17, 161, 18, and 162°, respectively (Table 3). This provides a corrected average tilt angle of ∼18°, in rather closer agreement with the observed 12° tilt by the branched chain glucoside than the high Gaussian-based estimates of average tilt angle from methods A and B (Table 2). However, we note the approximate nature of this estimate given the uneven profile of the distributions in some cases (most particularly, the *sn*-2 chain of βBCMal-$C_{12}C_{10}$).

Headgroup Structure. In each of the four simulated systems, the glycolipid headgroups are disaccharide moieties: β-maltose, β-cellobiose, and β-isomaltose. We first consider their flexibility. The $\varphi\psi$ distributions resulting from the MD simulations indicate that, for all four systems, the glycosidic angles explore only one low energy $\varphi\psi$ basin (Figure S5, Supporting Information). The distributions for βMal-C_{12}, βBCMal-$C_{12}C_{10}$, and βCel-C_{12} are similar in location and remain close to their crystallographic values. However, βIsoMal-C_{12} shifts from (−49°,167°) to a $\varphi\psi$ minimum at around (−130°,−55°). Due to its α-(1→6) linkage, βIsoMal possesses a third glycosidic torsion angle, ω, which describes rotation around the C5′–C6′ bond. In our simulation, this angle proved flexible, with its average value of 50° bounded by a standard deviation of ∼91°. We note that MD simulations have found the α-(1→6) linkage of isomaltose in aqueous solution to be more flexible than the α-(1→4) linkage of maltose.[54]

We next consider the polar interactions of the disaccharide headgroups. In theory, with each disaccharide possessing seven polar hydrogens able to donate a hydrogen bond and 11 oxygens able to accept 2 hydrogen bonds, the maximum possible number of hydrogen bonds a headgroup can make is 29. Unsurprisingly, simulations of 7 disaccharides in aqueous solution, including maltose, have observed far less than this idealized theoretical value, with 12–13 hydrogen bonds to water typically formed by the solute.[55] Here, given the significant orientational constraints of a thermotropic bilayer, besides the restriction of the steric bulk and covalent structure of the lipids themselves, the hydrogen bonding interactions between headgroups are fewer still. Indeed, we find that the total number of intermolecular hydrogen bonds formed between headgroups (i.e., both intra- and interlayer) range from 6.7 to 7.2 (Table 4). This value is approximately double that observed from thermotropic bilayer simulations of βGlc-C_8, where an average of only 3.5 total hydrogen bonds were formed per headgroup.[27] Interestingly, we observe that ∼55% of intermolecular hydrogen bonds formed are intralayer, except for the alkyl isomaltoside, where intra- and interlayer hydrogen bonds are formed in approximately equal proportions (Table 4, Figure 6e).

Table 4. Fractional Population of Hydrogen Bonds between Headgroups within a Layer (n_{intra}) and Both within and Across a Layer (n_{total})[a]

lipid	n_{intra}	n_{total}	T* (°C)	ref
βMal-C_{12}	3.9	7.2	245	56
βBCMal-$C_{12}C_{10}$	3.8	6.7	n/a	
βCel-C_{12}	3.8	7.2	208	57
βIsoMal-C_{12}	3.5	7.2	154, 157	57
βGlc-C_8	2.7	3.5	107	4

[a]Standard deviation varies between 0.10 and 0.15 hydrogen bonds. Literature values of clearing temperature (T^*) also reported, in °C.

It is also instructive to consider the distribution of intralayer hydrogen bonds as a function of oxygen sites around the sugar ring (Figure 6a–d). The distribution profiles for βMal-C_{12} and βBCMal-$C_{12}C_{10}$ are similar, both qualitatively and quantitatively (Figure 6a,b). In both cases, the greatest hydrogen bonding is predicted at O6 and O6′ of ∼0.8 bonds (see Figure 1 for atom labeling); there is also significant hydrogen bonding at O2′ and O3′ of the reducing sugar and O2 and O4 of the nonreducing sugar. Overall, however, the branched chain glycolipid makes half a hydrogen bond less on average, relative to its single chain counterpart (n_{total}, Table 4). The profile for βCel-C_{12} is broadly similar to βMal-C_{12}; the hydrogen bonding at O6 and O6′, although slightly less at ∼0.7 interactions, lies within a standard deviation of the βMal-C_{12} values (Figure 6c). Greater hydrogen bonding for βCel-C_{12} is seen at O2 and O3′ (Figure 6c) such that n_{total} remains ∼7 hydrogen bonds (Table 4). Interestingly, the β-(1→4) linkage of βCel-C_{12} appears to make these two proximal OH's (O2 and O3′) more available for interaction with the OH's of neighboring glycolipids. However, the distribution for βIsoMal-C_{12} is quite distinct from the other three systems (Figure 6d). Relative to βMal-C_{12}, βBCMal-$C_{12}C_{10}$, and βCel-C_{12}, the O6 of βIsoMal-C_{12} also makes ∼0.8 hydrogen bonds but now O1 (bonded to C6′) is largely unavailable for interaction due to its involvement in the α-(1→6) linkage (Figure 6d).

DISCUSSION

We have examined lamellar simulation models of four glycolipid systems, βMal-C_{12}, βBCMal-$C_{12}C_{10}$, βCel-C_{12}, and βIsoMal-C_{12}, exploring the effect on assemblage structure and dynamics of chain branching and different disaccharide headgroups. Considering first the effect of introducing a second, C_{10} alkyl chain into βMal-C_{12}, we observe an increased surface area per lipid (A) and an increased interlayer distance (d) (Table 1). Its bilayer spacing is comparable to Guerbet maltosides with $C_{12}C_8$ and $C_{14}C_{10}$ branched chains, where both have been confirmed by optical polarizing microscopy and X-ray studies to exhibit an L_α phase at room temperature.[37,53] This increase in A and d arises from the increased volume occupied by the additional chain, which is on average 75 Å^3 larger than for βMal-C_{12} (Table 1). The *sn*-1 and in particular

dx.doi.org/10.1021/jp302292s | J. Phys. Chem. B XXXX, XXX, XXX–XXX

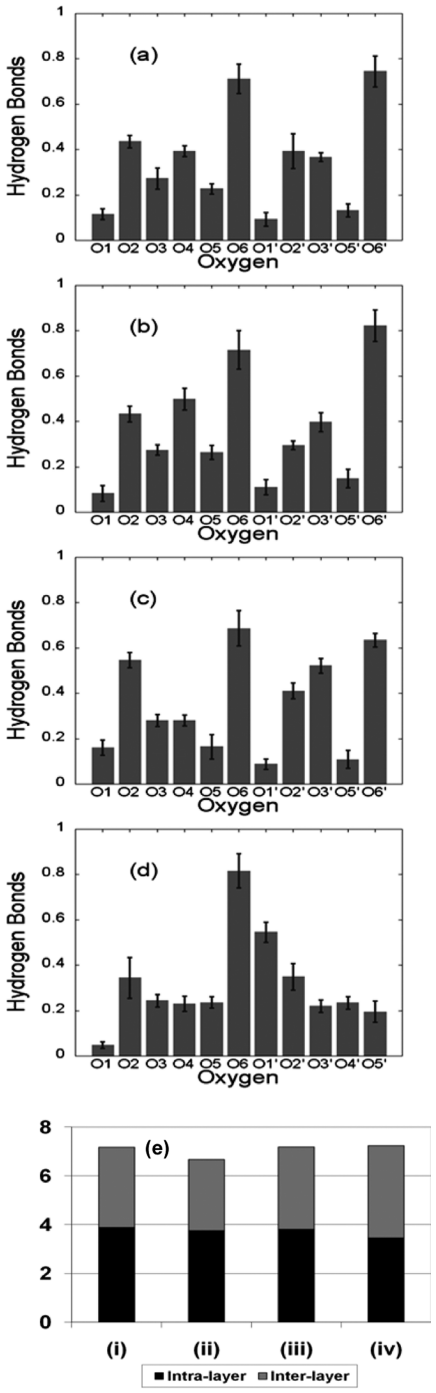

Figure 6. Intralayer hydrogen bond distribution over different oxygen locations (see Figure 1) for (a) βMal-C_{12}, (b) βBCMal-$C_{12}C_{10}$, (c) βCel-C_{12}, and (d) βIsoMal-C_{12}. (e) Total number of hydrogen bonds for (i) βMal-C_{12}, (ii) βBCMal-$C_{12}C_{10}$, (iii) βCel-C_{12}, and (iv) βIsoMal-C_{12}, comprised of interlayer (gray) and intralayer hydrogen bonds (black).

sn-2 chains of βBCMal-$C_{12}C_{10}$ are less ordered than the chain of dodecyl maltoside molecules. The average degree of tilt of the *sn*-1 chain is larger compared to that of βMal-C_{12} (Tables 2 and 3). However, the *sn*-2 chain is more highly tilted than both, also occupying a wide range of tilt angles (Figure S4, Supporting Information). The pattern of hydrogen bonding between headgroups is very similar for single and branched chain analogues; however, branching reduces the number of these hydrogen bonding interactions; this is possibly due to the greater packing constraints of increased steric congestion.

We also consider the effect of variation in disaccharide headgroup. βMal-C_{12} possesses an α-(1→4) linkage between its two glucosyl residues, whereas βCel-C_{12} is the β-(1→4) isomer. This configuration leads to subtly different predicted patterns in hydrogen bonding (Figure 6a,c) but approximately similar numbers of interactions between headgroups (Figure 6e, Table 4). Their chain regions appear comparable in structural and dynamic properties: for both, the chains are ordered (Figure 4). This observation supports numerous experimental observations that these glycolipids exist in an ordered lamellar phase (L_C) or gel phase (L_β) at room temperature.[4,57−59] Both chains also exhibit a maximum in order at their eighth carbon, a profile similar to that witnessed in simulations of other lipid bilayer systems.[23,24,47] For monosaccharide glycolipids, it has been suggested that the relative orientations of the C4 epimer and anomeric linkage influence the value of intralayer hydrogen bonding.[60] Thus, when these features are "cis" with respect to each other, as in the case of the alkyl β-galactoside and α-glucoside, the systems have higher clearing transitions, compared to those with a "trans" orientation, for example, alkyl α-galactoside and β-glucoside. Extending this idea to disaccharide lipids, we expect higher hydrogen bonding interactions for βCel-C_{12}, reflecting the trans−trans configurations, compared to βMal-C_{12} which has a cis−trans configuration. Our present investigation is unable to confirm this, but we note that, experimentally, the corresponding αMal-C_{12} (cis,cis)[61] and αCel-C_{12} (cis,trans)[59] have clearing transition temperatures of 205 and 224 °C, respectively, indicating that the above hypothesis is not unreasonable.

In this work, we find the most prominent difference in simulated properties on comparing βMal-C_{12} (or indeed βCel-C_{12}) with βIsoMal-C_{12}. The α-(1→6) linkage in the latter leads to significant changes in predicted bilayer properties: the surface area per headgroup is 10 Å^2 larger than for βMal-C_{12} or βCel-C_{12}, and the spacing d between layers is 18−19% less (Table 1). The ordering of the βIsoMal-C_{12} alkyl chain decreases monotonically toward its tip, as opposed to displaying a maximum around the eighth methylene (Figure 4). Indeed, the chain order parameter for βIsoMal-C_{12} is small, suggesting its hydrophobic region may not be in an ordered lamellar phase, as implied by the experimental studies reported previously.[57,59] The overall average tilt (Table 3) and its distribution (Figure S4, Supporting Information) are different for the regioisomers (1→6 vs 1→4 glycosidic bond), with a broader distribution seen for βIsoMal-C_{12}.

Due to the presence of an additional covalent bond in the glycosidic linkage of βIsoMal-C_{12}, significant differences in the hydrogen bonding pattern for regioisomers are also observed (Figure 6a,d). Indeed, a slight increase in interlayer hydrogen bonding of headgroups occurs (Table 4). This appears to arise from greater exposure of the disaccharide group, due to the extended structure of the 1→6 glycosidic linkage, and hence its larger surface area (Table 1). This C5′−C6′ bond is conformationally variable but also physically projects the nonreducing residue of the disaccharide headgroup further out from the chain region, making the headgroups more available for interaction. The alkyl chain is less ordered than in the corresponding (1→4)-linked malto- and cellobioside, and the interface region appears significantly undulated. Coiling of chain and undulation are consequences of increased surface area (Figure S2, Supporting Information), which places

dx.doi.org/10.1021/jp302292s | J. Phys. Chem. B XXXX, XXX, XXX−XXX

constraints on the packing of the alkyl chains. These rather large differences in simulated structure between βMal-C_{12} and βIsoMal-C_{12} are reflected in a marked difference in observed clearing temperature, on the order of 100 °C (Table 4). This much lower clearing temperature for βIsoMal-C_{12} is also reflected by the lower number of predicted intralayer hydrogen bonds formed by its bilayer assembly (Table 4).[27]

For the two different β-(1→4) linked glycolipids, we find that cellobioside has a higher chain order parameter of about 0.34 (Figure 4) compared to the corresponding α-(1→4)-linked maltoside (~0.25). This is a reflection of cellobiose's more linear ribbon-like structure compared to the bent shape of maltose, which gives rise to the helical turning in higher oligomers,[62,63] and thus influences chain order. This would suggest that the sugar groups pack more compactly in the cellobioside assembly compared to that of the maltoside. However, experimentally, the clearing transition temperature for maltoside (245 °C) is higher than that for the cellobioside (208 °C); see Table 4.[56,57] These observations suggest that extrapolation from tertiary homopolysaccharide structures is insufficient to account for the different clearing transitions of the glycosides.

Finally, we comment on the issue of chain orientation in the hydrophobic region. Previously, shorter chain monoalkyl glucopyranoside crystals have been reported as having head-to-head bilayer interdigitated chains or head-to-tail monolayers with no interdigitation.[64−67] Alternatively, many natural glycolipids are found to pack in a tilted and not interdigitated form.[68] Recent X-ray studies for longer chain length monoalkylated glycolipids[28] found the L_C phase to be both interdigitated as well as tilted. In addition, the Guerbet glycoside C_8 was also found to be in a tilted L_C phase, with an estimated tilt angle of ~12° from X-ray analysis.[53,69] The present glycolipid simulations also observe stable tilted chain orientations, ranging from 13 to 26° depending on headgroup. The tilt observed here is also comparable to that estimated from earlier bilayer simulations of decanoate (10°),[24] DPPC (~22°), and DPPE (19°).[15] This is also a similar finding to simulations of glycoglycerolipids containing glucosyl or galactosyl headgroups with phosphatidylcholine tails; there, tilt angles on the order of 19−20° were observed.[15]

It is interesting to consider the estimate of net chain tilt using method A. This method averages tilt over layers without correcting for leaflet orientation. For all of the glycolipids considered, the values of tilt via this method are around 90° (Table 2). Thus, each layer is tilting but there is no effective averaged tilt over a larger length scale, albeit here we only consider a four-layer glycolipid system. This may support previous claims of uncorrelated tilting in the hydrophobic region of glycolipids, due to the hydrophilic region acting as a barrier to transmission of tilt information;[61,70] this in turn could point to a possible low frequency relaxation process, found previously, for example, in the Goldstone mode in tilted smectic C monophilic liquid crystals. Larger simulation cells however are warranted to explore this aspect further.

CONCLUSIONS

Molecular dynamics simulations of anhydrous lamellae of βMal-C_{12}, βBCMal-$C_{12}C_{10}$, βCel-C_{12}, and βIsoMal-C_{12} have been employed to probe the molecular level consequences of chain branching and headgroup identity on assemblage structure and dynamics. Interestingly, while increased branching of the alkyl maltoside leads to measurable differences in the dimensions and dynamics of the assembly, the effects are rather less than the replacement of the maltosyl headgroup with an isomaltosyl moiety. The headgroup appears to play a crucial role in determining the microscopic properties of the glycolipid assemblies examined here; indeed, it is known that headgroup is a key determinant of thermodynamic behavior, as reflected by the clearing temperature, T^*.[5,9,60] Understanding the consequences of large or subtle changes in the covalent structure of glycolipids on their ensembles is a key step toward structure-based design of new glycolipid-based systems, as thermotropic and lyotropic materials suitable for a wide range of surfactant and thin film applications.[71]

ASSOCIATED CONTENT

Supporting Information

Table S1: The dihedral angles for the sugar units used in this simulation. Figure S2: Representative MD configurations (*xy* slice). Figure S3: Angular correlation between normalized molecular vectors S_i and the angle θ of the average tilt. Figure S4: Distribution of alkyl chain tilt angle θ as a function of glycolipid layer using method C. Figure S5: Ramachandran plots of φ (H1−C1−O1−C4′) and ψ (C1−O1−C4′−H4′). This material is available free of charge via the Internet at http://pubs.acs.org.

AUTHOR INFORMATION

Notes

The authors declare no competing financial interest.

ACKNOWLEDGMENTS

The authors would like to thank the University of Malaya and the Ministry of Higher Education High Impact Research Grant UM.C/625/1/HIR/MOHE/05 grant for supporting this project. Numerous computing resources from the University of Malaya, MIMOS, and the University of Manchester are acknowledged. R.H. and V.M.A. also thank Professors Wenbing Hu (Nanjing University) and Zhong-Can Ou-Yang (Institute of Theoretical Physics, CAS) for hosting them during the program "Growth of Hierarchical Functional Materials in Complex Fluids" at the Kavli Institute for Theoretical Physics China (KITPC), Institute of Theoretical Physics, Chinese Academy of Sciences (CAS) in Beijing, Jul 5−Aug 5, 2011.

REFERENCES

(1) Dembitsky, V. M. *Chem. Biodiversity* **2004**, *1*, 673−781.
(2) *Sugar based surfactants: Fundamentals and Applications*; Ruiz, C. C., Ed.; CRC Press: Boca Raton, FL, 2008; Vol. *143*.
(3) Balzer, D.; Lüders, H. H. *Nonionic Surfactants: Alkyl Polyglucosides*; Surfactant Science Series; Marcel Dekker: New York, 2000; Vol. *91*.
(4) Vill, V.; Bocker, T.; Thiem, J.; Fischer, F. *Liq. Cryst.* **1989**, *6*, 349−56.
(5) Hashim, R.; Sugimura, A.; Minamikawa, H.; Heidelberg, T. *Liq. Cryst.* **2012**, *39*, 1−17.
(6) Bujarski, J. J.; Hardy, S. F.; Miller, W. A.; Hall, T. C. *Virology* **1982**, *119*, 465−73.
(7) Lambert, O.; Levy, D.; Ranck, J. L.; Leblanc, G.; Rigaud, J. L. *Biophys. J.* **1998**, *74*, 918−30.
(8) Sasaki, T.; Demura, M.; Kato, N.; Mukai, Y. *Biochemistry* **2011**, *50*, 2283−90.
(9) Goodby, J. W.; Gortz, V.; Cowling, S. J.; Mackenzie, G.; Martin, P.; Plusquellec, D.; Benvegnu, T.; Boullanger, P.; Lafont, D.; Queneau, Y.; et al. *Chem. Soc. Rev.* **2007**, *36*, 1971−2032.

(10) Auvray, X.; Petipas, C.; Dupuy, C.; Louvet, S.; Anthore, R.; Rico-Lattes, I.; Lattes, A. *Eur. Phys. J. E* **2001**, *4*, 489−504.
(11) Lingwood, D.; Binnington, B.; Rog, T.; Vattulainen, I.; Grzybek, M.; Coskun, U.; Lingwood, C. A.; Simons, K. *Nat. Chem. Biol.* **2011**, *7*, 260−2.
(12) Chong, T. T.; Hashim, R.; Bryce, R. A. *J. Phys. Chem. B* **2006**, *110*, 4978−84.
(13) Hall, A.; Rog, T.; Karttunen, M.; Vattulainen, I. *J. Phys. Chem. B* **2010**, *114*, 7797−807.
(14) Konidala, P.; He, L.; Niemeyer, B. *J. Mol. Graphics Modell.* **2006**, *25*, 77−86.
(15) Róg, T.; Vattulainen, I.; Bunker, A.; Karttunen, M. *J. Phys. Chem. B* **2007**, *111*, 10146−54.
(16) Abel, S.; Dupradeau, F. Y.; Raman, E. P.; MacKerell, A. D., Jr.; Marchi, M. *J. Phys. Chem. B* **2011**, *115*, 487−99.
(17) Berendsen, H. J. *Science* **1996**, *271*, 954−5.
(18) Egberts, E.; Marrink, S. J.; Berendsen, H. J. *Eur. Biophys. J* **1994**, *22*, 423−36.
(19) Nguan, H. S.; Heidelberg, T.; Hashim, R.; Tiddy, G. J. T. *Liq. Cryst.* **2010**, *37*, 1205−13.
(20) Shinoda, W.; DeVane, R.; Klein, M. L. *J. Phys. Chem. B* **2010**, *114*, 6836−49.
(21) Shinoda, W.; Mikami, M.; Baba, T.; Hato, M. *J. Phys. Chem. B* **2004**, *108*, 9346−56.
(22) Tieleman, D. P.; Marrink, S. J.; Berendsen, H. J. *Biochim. Biophys. Acta* **1997**, *1331*, 235−70.
(23) Van der Ploeg, P.; Berendsen, H. J. C. *Mol. Phys.* **1983**, *49*, 233−48.
(24) Van der Ploeg, P.; Berendsen, H. J. C. *J. Chem. Phys.* **1982**, *76*, 3271−6.
(25) Rog, T.; Vattulainen, I.; Kartuttunen, M. *Cell. Mol. Biol. Lett.* **2005**, *10*, 92.
(26) Zhang, Z.; Bhide, S. Y.; Berkowitz, M. L. *J. Phys. Chem. B* **2007**, *111*, 12888−97.
(27) Chong, T. T.; Heidelberg, T.; Hashim, R.; Gary, S. *Liq. Cryst.* **2007**, *34*, 251−65.
(28) Ericsson, C. A.; Ericsson, L. C.; Ulvenlund, S. *Carbohydr. Res.* **2005**, *340*, 1529−37.
(29) Jeffrey, G. A. *Acc. Chem. Res.* **1986**, *19*, 168−73.
(30) *HyperChem(TM)*; Hypercube, Inc.: Gainesville, FL, 2003.
(31) IUPAC-IUB Commission on Biochemical Nomenclature. Abbreviations and symbols for the description of the conformation of polypeptide chains. Tentative rules (1969), *Biochemistry*, 1970/09/01 ed, **1970**, Vol. *9*, pp 3471-3479.
(32) McNaught, A. D. *Pure Appl. Chem.* **1996**, *68*, 1919−2008.
(33) Ott, K. H.; Meyer, B. *Carbohydr. Res.* **1996**, *281*, 11−34.
(34) Ham, J. T.; Williams, D. G. *Acta Crystallogr., Sect. B* **1970**, *26*, 1373−83.
(35) Jeffrey, G. A.; Huang, D. B. *Carbohydr. Res.* **1991**, *222*, 47−55.
(36) LiqCryst 4.2, Fujitsu FQS, Fukuoka, 2002, Database of Thermotropic Liquid Crystals, also available from http://liqcryst.chemie.uni-hamburg.de.
(37) Hashim, R.; Hashim, H. H. A.; Rodzi, N. Z. M.; Hussen, R. S. D.; Heidelberg, T. *Thin Solid Films* **2006**, *509*, 27−35.
(38) *AMBER 9*; University of California: San Francisco, 2006.
(39) Hornak, V.; Abel, R.; Okur, A.; Strockbine, B.; A., R. *Proteins* **2006**, *65*, 712−25.
(40) Kirschner, K. N.; Yongye, A. B.; Tschampel, S. M.; Gonzalez-Outeirino, J.; Daniels, C. R.; Foley, B. L.; Woods, R. J. *J. Comput. Chem.* **2008**, *29*, 622−55.
(41) Darden, T.; York, D.; Pedersen, L. *J. Chem. Phys.* **1993**, *98*, 10089−92.
(42) Essmann, U.; Perera, L.; Berkowitz, M. L.; Darden, T.; Lee, H.; Pedersen, L. G. *J. Chem. Phys.* **1995**, *103*, 8577−93.
(43) Miyamoto, S.; Kollman, P. A. *J. Comput. Chem.* **1992**, *13*, 952−62.
(44) Andrea, T. A.; Swope, W. C.; Andersen, H. C. *J. Chem. Phys.* **1983**, *79*, 4576−84.
(45) Kapla, J.; Stevensson, B.; Dahlberg, M.; Maliniak, A. *J. Phys. Chem. B* **2011**, *116*, 244−52.
(46) Saupe, A. *Z. Naturforsch., A: Phys. Sci.* **1964**, *19*, 161−71.
(47) Essex, J. W.; Hann, M. M.; Richards, W. G. *Philos. Trans. R. Soc. London, Ser. B* **1994**, *344*, 239−60.
(48) Tieleman, D. P. Personal communication. Discussion on "Monitoring the equilibrium condition for lipid bilayer simulation" is gratefully acknowledged.
(49) Lim, J. B.; Klauda, J. B. *Biochim. Biophys. Acta, Biomembr* **2011**, *1808*, 323−31.
(50) Moore, P. B.; Lopez, C. F.; Klein, M. L. *Biophys. J.* **2001**, *81*, 2484−94.
(51) Trouard, T. P.; Nevzorov, A. A.; Alam, T. M.; Job, C.; Zajicek, J.; Brown, M. F. *J. Chem. Phys.* **1999**, *110*, 8802−18.
(52) Nevzorov, A. A.; Trouard, T. P.; Brown, M. F. *Biophys. J.* **1999**, *76*, A441-A.
(53) Hashim, R.; Hamid, H. A. A.; Seddon, J. M.; Brooks, N. J.; Heidelberg, T.; Zahid, N. M.; Mirzadeh, S. M. "Mesophase Structure Investigation of Branched Chain Glycosides"; 3rd International Symposium on the Manipulation of Advanced Smart Material, 2010, Osaka, Japan.
(54) Best, R. B.; Jackson, G. E.; Naidoo, K. J. *J. Phys. Chem. B* **2001**, *105*, 4742−51.
(55) Cheetham, N. W. H.; Dasgupta, P. *Aust. J. Chem.* **2005**, *58*, 803−9.
(56) Marcus, M. A. *Mol. Cryst. Liq. Cryst. Sci. Technol., Sect. A* **1986**, *3*, 85−9.
(57) Koeltzow, D. E.; Urfer, A. D. *J. Am. Oil Chem. Soc.* **1984**, *61*, 1651−5.
(58) Hori, R. *Yakugaku Zasshi* **1958**, *78*, 999.
(59) Vill, V. Ph.D. Dissertation, University of Munster, 1990.
(60) Hashim, R.; Mirzadeh, S. M.; Heidelberg, T.; Minamikawa, H.; Yoshiaki, T.; Sugimura, A. *Carbohydr. Res.* **2011**, *346*, 2948−56.
(61) Vill, V.; Bocker, T.; Thiem, J.; Fischer, F. *Liq. Cryst.* **2006**, *33*, 1353−8.
(62) Hato, M. *Curr. Opin. Colloid Interface Sci.* **2001**, *6*, 268−76.
(63) Hato, M.; Minamikawa, H.; Tamada, K.; Baba, T.; Tanabe, Y. *Adv. Colloid Interface Sci.* **1999**, *80*, 233−70.
(64) Jeffrey, G. A. *Acta Crystallogr., Sect. B: Struct. Sci.* **1990**, *46* (Pt 2), 89−103.
(65) Jeffrey, G. A.; Rosenstein, R. D. *Adv. Carbohydr. Chem. Biochem.* **1964**, *19*, 7−22.
(66) Jeffrey, G. A.; Ruble, J. R.; Sepehrnia, B. *Carbohydr. Res.* **1985**, *144*, 197−203.
(67) Jeffrey, G. A.; Yeon, Y.; Abola, J. *Carbohydr. Res.* **1987**, *169*, 1−11.
(68) Abrahamsson, S.; Dahlen, B.; Pascher, I. *Acta Crystallogr., Sect. B: Struct. Sci.* **1977**, *33*, 2008−13.
(69) Brooks, N. J.; Hamid, H. A. A.; Hashim, R.; Heidelberg, T.; Seddon, J. M.; Conn, C. E.; Husseini, S. M. M.; Zahid, N. I.; Hussen, R. S. D. *Liq. Cryst.* **2011**, *38*, 1725−34.
(70) Abeygunaratne, S.; Hashim, R.; Vill, V. *Phys. Rev. E* **2006**, *73*, 011916.
(71) Wai Ling, K.; Wee Chen, G.; Wan Haliza Abd, M.; Rauzah, H.; Thorsten, H. *Thin Solid Films* **2010**, *518*, 4412−6.